

Nearshore Monitoring with X-Band Radar: Maximising Utility in Dynamic and Complex Environments

John Atkinson¹, Luciana S. Esteves², Jon Williams³, Paul Bell⁴, and David L McCann⁴

¹Ørsted UK

²Bournemouth University

³Mott MacDonald

⁴National Oceanography Centre

November 22, 2022

Abstract

Data quantifying the nature and range of bathymetric changes in the near-shore are required for coastal management and engineering works. However, due to high costs and complex logistics, bathymetric surveys are usually infrequent. This study demonstrates that ground-based X-band radar offers a cost-effective alternative to monitor seabed changes at relatively high frequency and over large near-shore areas. Through a robust data processing and quality control framework developed to validate radar-derived data and quantify uncertainties, bathymetric maps were obtained using an 18-month radar installation at Thorpeness, U.K. The analysis incorporates calibration of water levels and wave heights; validation of radar-derived water depth using concurrent multibeam surveys; the application of a method to reduce the influence of data scatter and outliers; and assessment of spatio-temporal variability of data quality due to varying wave heights and direction. For conditions when the wave height is >1 m, and the angle of wave approach relative to the radar is relatively small, the accuracy of the radar-derived depths is shown to be $\{\text{plus minus}\}0.5$ m at 40×40 m spatial resolution. At Thorpeness, quantification of changes exceeding this error was possible at time-scales as short as three weeks, and near-shore volume changes are seen to be of a comparable magnitude to historical longshore transport rates in the area. The use of radar can provide to coastal managers an early warning of changes in offshore bathymetry likely to impact vulnerable coastal locations; thereby allowing mobilisation of resources that may be required to protect lives and property.

Nearshore Monitoring with X-Band Radar: Maximising Utility in Dynamic and Complex Environments

John Atkinson^{1*}, Luciana S. Esteves¹, Jon J. Williams², Paul S. Bell³, and David L. McCann³

¹ Faculty of Science & Technology, Bournemouth University, Poole, UK.

² Ports, Coastal & Offshore, Mott MacDonald Ltd, Croydon, UK.

³ National Oceanography Centre, Liverpool, UK.

Corresponding author: Luciana S. Esteves (lesteves@bournemouth.ac.uk)

*Current affiliation: Ørsted UK, Howick place, London, UK

Key Points:

- Weekly and monthly changes in near-shore bathymetry at a complex site were quantified for 18 months at using a marine X-band radar.
- Measurement uncertainties were quantified using a robust data processing and quality control framework.
- Temporal bathymetric changes over 3 weeks were of similar magnitude to those observed over 6 months and showed the key role of bi-directional waves.

Abstract

Data quantifying the nature and range of bathymetric changes in the near-shore are required for coastal management and engineering works. However, due to high costs and complex logistics, bathymetric surveys are usually infrequent. This study demonstrates that ground-based X-band radar offers a cost-effective alternative to monitor seabed changes at relatively high frequency and over large near-shore areas. Through a robust data processing and quality control framework developed to validate radar-derived data and quantify uncertainties, a series of bathymetric maps were obtained using an 18-month radar installation at Thorpeness, U.K. The analysis incorporates calibration of water levels and wave heights; validation of radar-derived water depth using concurrent multibeam surveys; the application of a method to reduce the influence of data scatter and outliers; and assessment of spatio-temporal variability of data quality due to varying wave heights and direction. For conditions when the wave height is >1 m, and the angle of wave approach relative to the radar is relatively small, the accuracy of the radar-derived depths is shown to be ± 0.5 m at 40×40 m spatial resolution. At Thorpeness, quantification of changes exceeding this error was possible at time-scales as short as three weeks, and near-shore volume changes are seen to be of a comparable magnitude to historical longshore transport rates in the area. The use of radar can provide to coastal managers an early warning of changes in offshore bathymetry likely to impact vulnerable coastal locations; thereby allowing mobilisation of resources that may be required to protect lives and property.

1 Introduction

Being able to accurately and consistently monitor beach and near-shore processes provides the foundation for understanding beach dynamics (Davidson et al., 2007). The control on waves by changing near-shore bathymetry has been the subject of increased research interest, primarily to understand and predict shoreline changes (Hequette et al., 2009; Hequette and Aernouts, 2010; Lazarus & Murray, 2011; Ruessink et al., 2004; Stokes et al., 2015). Near-shore sediment accretion provides protection to the coast during the first high energy events that follow periods of low energy (Dissanayake et al., 2015). Conversely, coastal erosion hotspots have been attributed to the concentration of wave energy caused by complex near-shore geology (Browder and McNinch, 2006; Burningham and French, 2017; Schupp et al., 2006; Williams et al., 2019). These processes are controlled further by changes in the incident wave climate (Hegermiller et al., 2017; Lazarus & Murray, 2011) particularly wave direction bimodality (Burningham and French, 2016, 2017; Williams et al., 2019).

Quantifying magnitudes of coastal change and understanding drivers of temporal and spatial variability is required to inform coastal management decisions (Atkinson & Esteves, 2018; Pye & Blott, 2006; Smit et al., 2007). Coastal researchers and managers increasingly need to employ a range of techniques to conceptualise site-specific morphodynamic behaviour. Although technology advances enabled more accurately monitoring of beach changes and over large areas (Burvingt et al., 2017), challenges persist regarding quantifying bathymetric changes in the near-shore (Kotilainen & Kaskela, 2017; Pacheco et al., 2015).

Measurements of near-shore waves, hydrodynamics and the seabed require expensive *in situ* installations of sensors that have limited spatial coverage (e.g. current meters and wave buoys) and deployment from vessels (e.g. multibeam surveys), which have limitations in shallow waters (Costa et al., 2009). Remote sensing methods are often constrained by the sensors' ability to 'see' at times of unfavourable weather or water conditions during storms or high energy

events, exactly when largest near-shore changes are expected to occur. Bathymetric Light Detection and Ranging (LiDAR) and satellite sensors can be used in areas of minimal water turbidity but show large errors where water transparency is low and in areas of breaking waves (Chust et al., 2010; Costa et al., 2009; Kotilainen & Kaskela, 2017). While results obtained from multispectral Dove satellites imagery showed vertical root-mean-square error between 1.22 and 1.86 m for depths of 4 to 10 m at 4 m spatial resolution based on best cloud-free and minimal turbidity conditions (Li et al., 2019), the temporal resolution and accuracy of satellite imagery remain limited by cloud cover.

Video systems, such as Argus (Aarnikhof & Holman, 1999; Holman et al., 1993; Holman & Stanley, 2007; Kroon et al., 2007; Smit et al., 2007) have been used to derive water depths and basic wave and current parameters (Holman et al., 2013), changes in shoreline position (Kroon et al., 2007), understand surf zone bar dynamics (Masselink et al., 2014) and intertidal changes (Davidson et al., 2007; Smit et al., 2007). The use of video systems is limited by daylight hours and weather-related visibility and requires image rectification and geometric corrections if cameras move due to wind or other factors. Further, these systems have a limited field of view (maximum 1000-1500 m per camera) and pixel resolution increases with distance, exceeding 40m at 1500 m from the camera (Holman and Stanley 2007). Radar offers an alternative to optical and passive remote sensing, with the benefits of capturing data irrespective of daylight and weather conditions, not requiring image correction, and having a larger field of view. Analysis of X-band radar images of the sea surface can derive information of bathymetry, waves and surface currents over an area of 4-5 km radius (Bell et al., 2011; McCann & Bell, 2014; Bell et al., 2016).

X-band radar as a remote sensing tool relies on the presence of backscatter known as ‘sea clutter’, referring to spatially and temporally periodic backscatter signals directly related to ocean surface waves. Through a frequency domain analysis (e.g. Fourier transform) the spectral characteristics of ocean surface waves can be inferred, and from these, wave parameters such as frequency and wavelength can be calculated. The use of these calculated wave parameters to infer hydrographic properties using the physics of dispersive waves is known as ‘wave inversion’ and is well-established with X-band radar (Bell, 1999; Hessner and Bell, 2009; Ludeno et al., 2015, Lund et al., 2020). Most recently, cBathy (Holman et al., 2013) has been applied to derive near-shore bathymetric information from both camera images and radar data (Honegger et al., 2019; Honegger et al., 2020; Gawehn et al., 2020). However, the application of radar-derived bathymetry to understand near-shore change has been limited so far. This paper applies a robust data quality analysis to quantify uncertainties and demonstrate that radar-derived bathymetry can be used to estimate changes in water depth and sediment volume in near-shore areas. The radar data analysed here were obtained from an 18-month deployment at Thorpeness, a site on the east coast of the U.K. with complex underwater geology and exposure to a bimodal wave climate. In recent years, the site has been subject to episodic coastal erosion that threatens a number of residential dwellings, and the beach and near-shore region are thought to be particularly dynamic at this location. The project sought to advance knowledge of this site by assessing the viability of X-band radar as a coastal monitoring tool.

2 Study Site

The radar was installed on a cliff top at the north end of Thorpeness village (52.182°N, 1.613°E, Suffolk, East England). The site is characterised by a mixed sand and gravel coast with

a prominent cusped gravel foreland (locally called the ness) to the north (Figure 1). The site is exposed to a semi-diurnal mesotidal regime (peak astronomical range ~ 2.5 m) and is susceptible to storm surges exceeding 2 m when water levels can reach 3.78 m above Ordnance Datum Newlyn, ODN (Wadey et al., 2015). The offshore wave climate (based on the Cefas WaveNet West Gabbard buoy, 51.952°N 002.109°E , 41 m depth) shows bimodal direction, with the peak direction (DirP) oscillating between S.W. and N.E., varying in duration and energy year to year and within the years, although not reflecting a strong seasonal signal (Atkinson and Esteves, 2018).



Figure 1. Aerial view of the X-band radar installation site at the north end of the Thorpeness village, Suffolk (U.K.).

The beach morphology shows high temporal and spatial variability and is controlled by underwater geology and bimodal wave direction, and influenced by coastal protection works (Atkinson and Esteves, 2018). The near-shore is characterised by mobile banks, and complex underlying hard geology with underwater ridges 12 km long and 2 km wide extend SW-NE offshore from the coast. These ridges are formed by the Pliocene Coralline Crag formation comprising cemented fine sands and silts (Long and Zalasiewicz, 2011). A dynamic near-shore seabed feature south of the ness has been shown to respond to the bimodal wave direction (Atkinson et al., 2018) and modelling simulations indicate the feature contributes in part to the occurrence of episodic erosion hotspots along the Thorpeness village frontage (Williams et al., 2019). Similar effects of near-shore banks were observed elsewhere along the Suffolk coast (Burningham & French, 2016).

3 Materials and Methods

A Kelvin Hughes 10kW, 9.41 GHz marine X-band radar system was deployed at Thorpeness in August 2015. The 2.4 m horizontally polarised antenna had a mean rotation time of ~2.6 seconds and had a 3dB horizontal beamwidth of ~0.8-degrees. The radar transceiver and antenna were installed on a 12m high scaffold tower on a cliff top overlooking the study area, at a total elevation of approximately 20 m above mean sea level (Figure 1). The study focused on an area of 3.3 km² (1.5 km alongshore x 2.2 km offshore). The radar video signal was digitised using the WaMoS II analogue-to-digital converter (OceanWaveS GmbH) in ‘B-scan’ polar coordinate format at 1/3 degree azimuthal and 5 m range resolution. WaMoS II is a well-established commercial system used to measure sea state conditions from X-band radar data following algorithms well documented in the literature (Hessner et al., 2015, 2014; Reichert et al., 1999; Wyatt et al., 2003). This software was used to derive wave spectral parameters from radar data, including significant wave height (H_s), peak wave period (T_p), mean wave period (T_m), mean wave direction (DirM) and peak mean direction (DirP).

The ‘B-scan’ polar-coordinate radar imagery was compressed, and scan converted via bi-linear interpolation to Cartesian coordinates (OSGB36) for storage and analysis. Data were collected between 16-Sep-2015 and 18-Apr-2017. The radar was set up to record data for 11 minutes (256 rotations, 2.63 seconds per rotation) every 30 minutes; generating a time-series ‘image stack’ (sweeps of the radar). These image stacks were then pre-processed automatically on-site to remove non-uniformities in the antenna rotation rate due to wind effects and produce a final uniform angular resolution of three pulses per degree to reduce the files sizes stored on an internal hard drive. These files were downloaded during site visits and processed off-site for the production of bathymetric maps.

3.1 Estimating water depth

Bathymetric maps were produced from radar data using the bathymetric inversion algorithms based on the linear wave theory (Borge et al. 2004; Bell, 1999; Bell & Osler, 2011):

$$\omega = \sqrt{gk \tanh(kh)} + u \cdot k \quad 1$$

where ω is angular wave frequency, g is the acceleration due to gravity, k is the wavenumber, h is the mean water depth, and u is the surface current velocity. Within a region defined by ω , the mean water depth directly affects k . To calculate the wave parameters, the analysis employs a 3-D Fast Fourier Transform (FFT) over a finite water surface area (the ‘analysis window’). This must be large enough to cover at least one wavelength in all directions and assumes that the area within the analysis window is homogenous with respect to both k and frequency spectra. The commonly used 3D FFT approach is applied to the analysis window time stack of image data. As FFT methods inherently allow the identification of integer numbers of waveforms in each dimension, this can lead to a lack of precision in identifying precise wavelengths in small analysis windows that contain low numbers of waves. To mitigate this, the 3D FFT was augmented using a Phase-Locked Loop type algorithm that can precisely identify the dominant 2D wavelength signal at each wave frequency (Bell & Osler, 2011). Crucially, a wave inversion method can only function with enough wavelengths within the analysis window to, at a minimum, satisfy the Nyquist frequency of the longest, lowest-frequency waves present at the time. In practice, this results in a minimum analysis window size of 150–200m depending on

local conditions. To create a spatial map of calculated hydrographic parameters, the analysis window is stepped spatially with the parameters calculated for the centre of the box. An important consideration is the assumption of homogeneity within the analysis window.

Often, for simplicity, underlying current effects are assumed to have a minimal effect on the wave propagation (Honegget et al., 2019). Although current magnitudes at the present site are not extreme when compared to studies incorporating current analysis (e.g. McCann and Bell, 2014 in a tidal race peak flow of 3.5 m s^{-1}), the local tidally-induced currents exceed 1.5 m s^{-1} (Lees, 1983) and waves often approach the coast at an oblique angle implying the potential for a significant wave-current interaction. Therefore, to undertake a robust bathymetric inversion, a current correction factor needs to be employed. In this case, the current correction technique of Hessner and Bell (2009) and based on Senet et al. (2001) was applied. This utilises analysis of Doppler shift effects on k , which increases or decreases wave frequency dependent on the direction of the current flow. The surface current is obtained by calculating the Doppler shift for each wavenumber within each analysis window.

Incorporating the depth and current analysis within each analysis window provides an ‘instantaneous’ estimation of the water depth as a probability density function (PDF) for each image stack. The peak of the PDF describes the ‘most probable depth’ at a point centred in the analysis window. In real-world conditions, these instantaneous measurements are generally noisy on an individual basis and if averaged in isolation, are very likely to introduce a bias to the final result. An average of sequential PDFs for a given geographic position (analysis window) can be taken to mitigate this bias. The aim is to average out the noise of the individual probability functions and allow a more representative ‘most probable depth’ to be determined. By taking this approach, a number of individually noisy results combine to generate a more stable PDF for the water depth from which the most likely depth (the peak of the distribution) can be obtained. However, the calculation also needs to allow the sea bed to evolve over time. This is achieved through either (a) a windowing function, or (b) by allowing each PDF to decay in importance with time in the manner of a radioactive half-life. This technique is used in this paper and is hereafter termed the *depth-memory*.

In the *depth-memory* approach, an integration half-life time is defined in terms of the number of records (R_n). When the approach is first initialised on a new site, each new probability function for a given geographic location is corrected for the tide level. This ensures that depths are relative to the chosen datum. The records are then added together until the defined consecutive R_n value is reached. If R_n is set to 10, record 1 makes up $1/10$ (0.1) of the total PDF

after the tenth record is reached. In this case, records 1 to 10 are defined as the *depth-memory* stabilisation period so that:

- After 11 records, record 1 makes up $(1/10)*(1-1/10) = 0.090$ of the total;
- After 12 records, record 1 makes up $0.09*(1-1/10) = 0.081$ of the total; and
- After 13 records, record 1 makes up $0.081*(1-1/10) = 0.073$ of the total and so on.

After approximately 20 records, the influence of record number 1 to the integrated probability density function has halved to $1/20$. By 32 records it has decayed to less than $1/100$, and by record 54, it has decayed to less than $1/1000$.

The selected value for R_n is highly dependent on the activity of the seabed. At sites where the seabed is immobile, a large R_n value can be defined and a long term, stable bathymetric map can be derived. At sites where the seabed is mobile and complex, a shorter R_n value is required to prevent previous records dominating the average and a change 'lag' occurring (i.e. the depth memory is continually catching up with the present state). The approach used to define the most appropriate R_n value for the present site is described below.

3.2 Tidal Correction

To relate radar-derived depth to a datum and to allow averaging over consecutive records, the algorithms require tidal elevation data that include astronomical and metrological forcing. This can be provided from a tide gauge or through a 'synthetic' tide approach, in which a residual value from a nearby tide gauge can be added to a harmonic prediction at the site (e.g. Bell et al., 2016)

In this study, a synthetic tide approach used data from a pressure sensor deployed within a drainage sluice at a location 2 km south of Thorpeness for 3 months between 27-Apr-2016 and 31-Jul-2016. The elevation of the pressure sensor within the sluice was approximately the half-tide level, so only data for water levels above this were able to be used for the comparison. These data allowed calibration of observed water levels against (a) a synthetic tide derived from residuals from a permanent Class 1 tide gauge at Lowestoft, U.K. (45 km north of Thorpeness); and (b) POLPRED harmonic prediction (NOC, 2019) close to the radar deployment field site. A good agreement was obtained between the measured and synthetic tidal time-series (Figure 2a). After applying the Lowestoft tidal residual value to the astronomical predictions (Figure 2b, c) the correlation coefficient R^2 increased from 0.75 to 0.96.

3.3 Wave height calibration

Due to the nonlinearity of the radar imaging mechanism, wave height cannot be inferred directly from the raw data (Borge et al., 1999). However, a calibration can be applied to the radar data using coincident wave measurements from another instrument (Alpers & Hasselmann, 1982). Here, significant wave height, H_s , time-series from the Cefas wave buoy located ~1900 m

north and ~3500 m east of the radar were used to calibrate the radar-derived wave height (Figure 2d) using the relationship:

$$H_s = A + B \sqrt{SNR}$$

2

where A is the intercept and B the slope of the fit between the Signal-to-Noise Ratio of the dispersion relation fit (SNR, calculated by the WaMoS II software). The resulting calibrated H_s relationship has been used subsequently in the radar data quality control process described in the following sections.

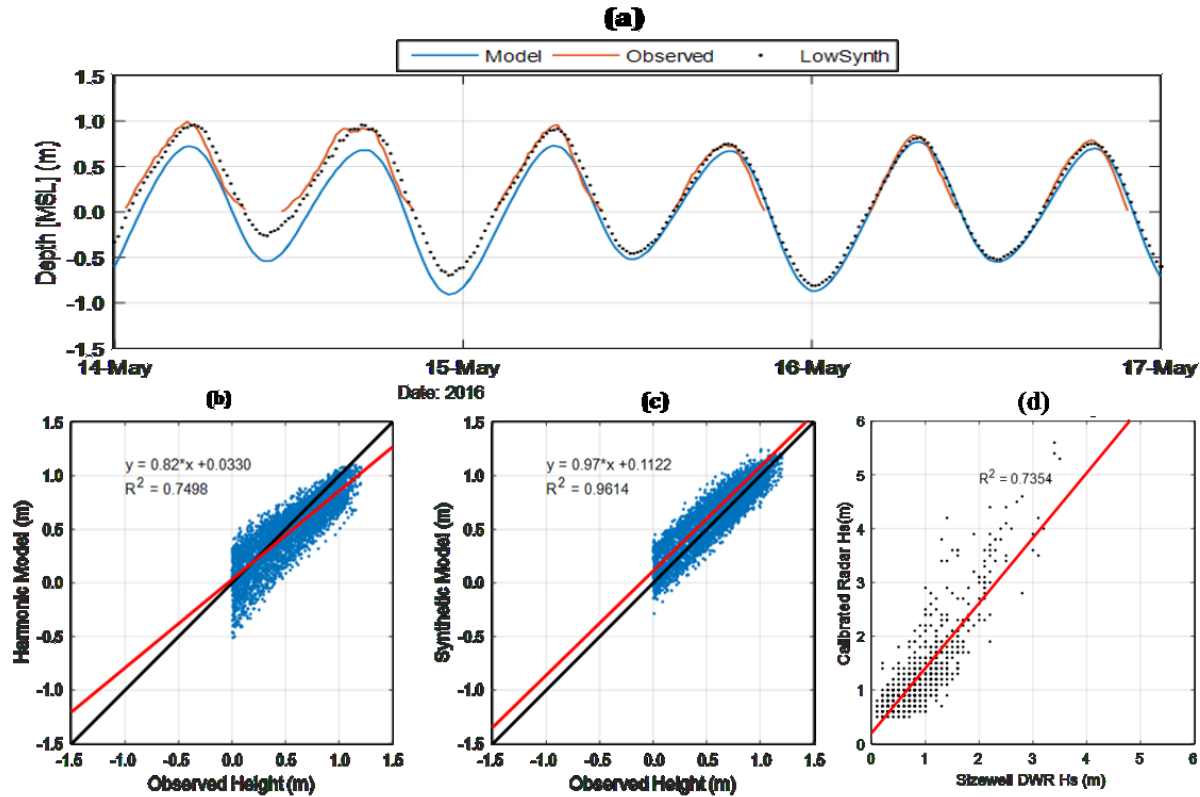


Figure 2. (a) Three-day window where the synthetic tide model (Lowestoft) was seen to perform well against the data recorded within the sluice. (b) RMS analysis of harmonic model and (c) synthetic model against observed water level >0 m only to reflect restricted fluctuations at the location of the pressure sensor deployment. (d) Calibrated radar-derived wave height against Sizewell directional Waverider data.

3.4 Spatial resolution of the radar-derived bathymetry

After optimisation against measured bathymetry, the bathymetric analysis of the radar data used a 160x160 m window that was shifted in 40 m increments throughout the radar field-of-view, resulting in a 40x40 m bathymetry grid (**Error! Reference source not found.**). Although this grid size is smaller than would be generally recommended for this type of analysis, it enabled resolution of seabed changes and features of interest. In real-world environments (rather than synthetic data), several wavelengths are required within an analysis window to obtain a good measure of the wavelength at any given wave frequency using the combined FFT and PLL method. The window size acts inherently as a low pass filter on the detected bathymetry, and the choice of window size is a trade-off at each site between the bathymetric

resolution needed for the application and the noise level that tends to increase with smaller window size. It must be noted that this analysis window size and step length are at the extreme end of what is routinely possible using this type of wave inversion analysis on real-world data. Better performance by a variety of methods is possible with high-quality raw data recorded under ideal conditions, but such events in most locations are the exception rather than the rule. It is possible to use an analysis window as small as 160m in this case due to the predominantly high frequency and thus short wavelength of waves at the site, shallow depths, favourable wave direction with respect to the radar beam and the relatively high elevation of the radar antenna with respect to the ocean surface.

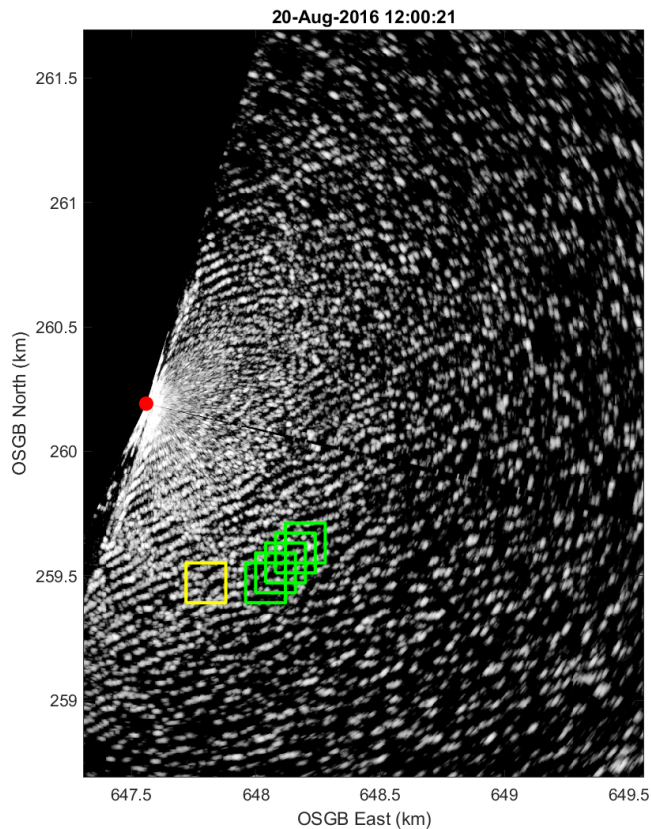


Figure 3. An example of the 160x160 m analysis window (yellow) and the 40m step length (green) used in wave-inversion calculations to infer the water depth overlaid on a raw backscatter image showing waves approaching from the S.E.

3.5 Depth-memory stabilisation

When defining the *depth-memory* record length (R_n) the interplay between R_n , the processing resolution and wave climate needs to be established. The impact of wave climate is shown from two starting points selected within 72 hours of each other (Figure 4): Scenario 1 (09-Oct-2019 0000 to 1130) occurred during low wave energy ($H_s < 1\text{m}$) with variable peak direction

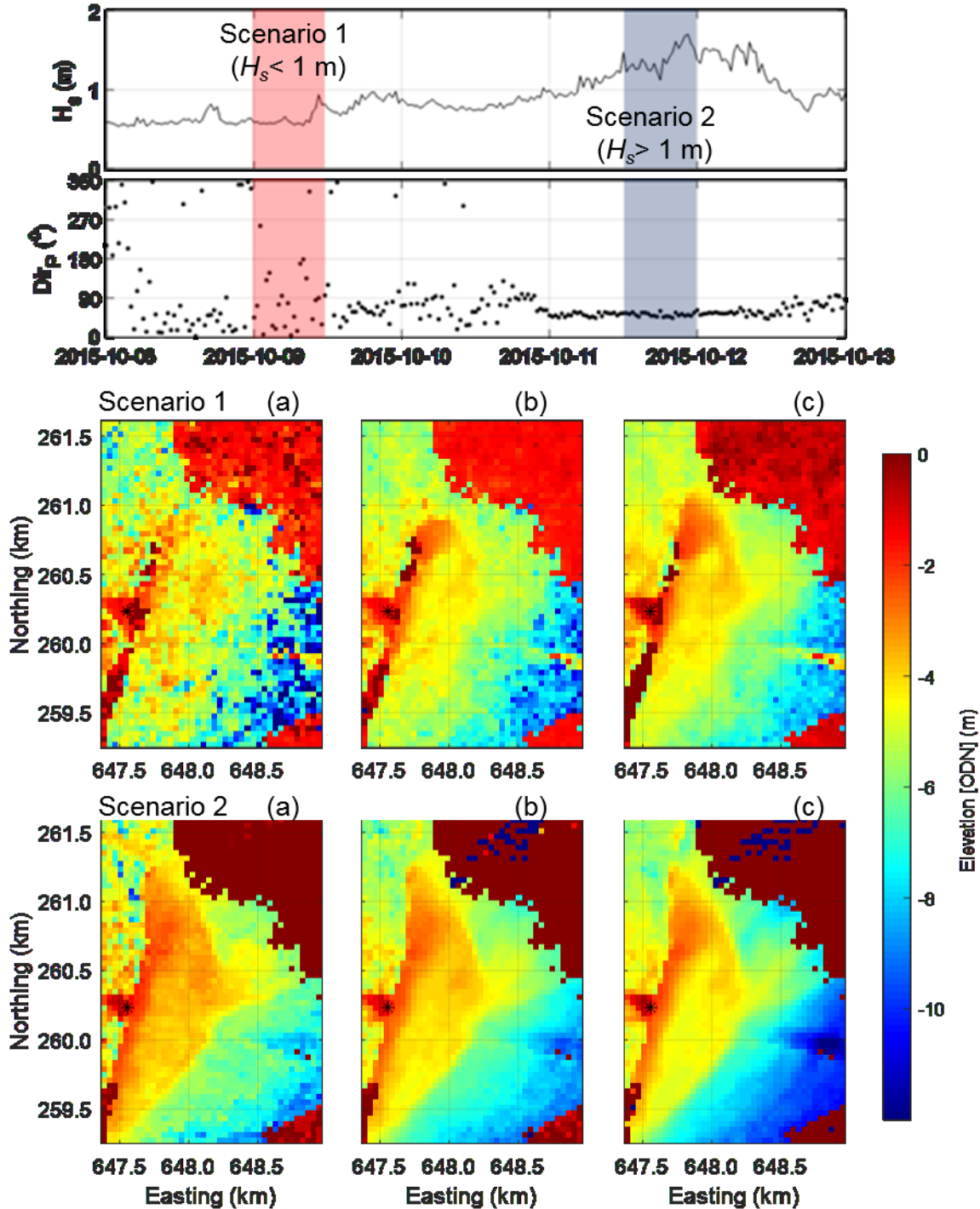


Figure 4. Time-series (top panel) of significant wave height (H_s) and peak wave direction (DirP) identifying two 12-hour (24 records) periods used to demonstrate the effects of the depth memory for low (Scenario 1) and moderate (Scenario 2) wave conditions on derived bathymetric maps at (a) record 1, instantaneous map, (b) record 6, 3 hours, and (c) record 24, 12 hours. Radar position is indicated by the black star.

(DirP) indicative of a low energy sea; Scenario 2 (11-Oct- 2015 1200 to 2330) occurred during moderate wave heights ($H_s = 1.25$ to 1.8 m) with a sustained northerly DirP. The derived bathymetric maps after 1, 6 and 24 records (30 minutes, 3 and 12 hours respectively, Figure 4)

show that both Scenario 1 (top row, 1a-1c) and 2 (bottom row 2a-2c) begin to show distinct bathymetric features. However, the low wave height of Scenario 1 is shown to take longer to develop and after 24 records still shows considerable variability. When this is compared to Scenario 2, the first record shows the distinct bathymetry of the area, which is steadily refined over the following 24 records.

During low wave heights, the data processing algorithms struggled to define wave parameters and to apply an accurate wave inversion. This lower limit for the wave height of detectable waves is a well-known effect for all types of radar remote sensing and is generally quoted as between H_s values of 0.5 m and 1 m – below which there is insufficient sea surface roughness to create detectable sea-clutter backscatter on radar data. As a consequence, there was uncertainty in depth estimations, and longer R_n values were required to produce a stable bathymetric map. After 24 low wave height records the shape of the near-shore is less well defined than after 6 records when wave heights exceeding 1 m. However, since wave heights less than 1 m combined with the relatively low tidal currents at the site result in low rates of bedload sediment transport and small bathymetric changes, these conditions are of little interest in the present study. The analysis therefore focused exclusively on periods when wave height consistently exceeded a 1 m H_s threshold for the period defined by R_n .

3.6 Radar-derived water depth validation

Bathymetric data from a multibeam survey conducted in January 2017 were used to validate the accuracy of radar-derived bathymetry. These survey data were resampled at the same spatial resolution as the step length of the radar wave inversion (Atkinson et al., 2018).

3.7 Data quality control framework

Irrespective of *depth-memory* length, spatial resolution and wave climate, the radar data had several limitations including (a) tidal effects causing variable data quality in shallow cells at the shoreline; (b) blocking of the radar view by the ness; and (c) some mechanical issues with the

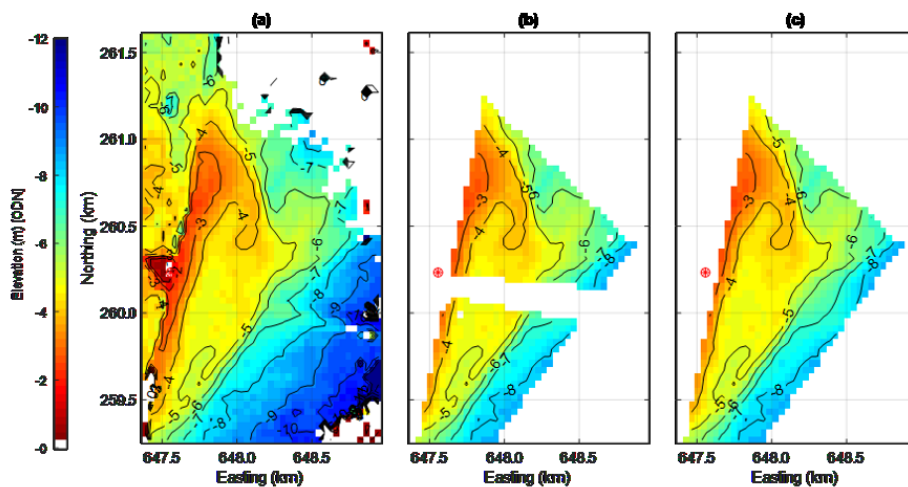


Figure 5. (a) Radar-derived bathymetric map (12-Oct-2015 00:00) and stages of quality control. (b) Removal of areas of poor data caused by a mechanical issue and the highly variable data due to depth and range. (c) Natural neighbour interpolation was used to fill the data gap across the radar view. Radar position indicated by the red circle.

radar during the deployment. These artefacts were removed through a data screening process to establish the regions of low data quality and return (Figure 5a). While the majority of the data were corrected and realigned automatically, some losses occurred (Figure 5b) and missing data were replaced by interpolation using the natural neighbour method (Sibson 1981; Figure 5c). This data quality control allowed identifying an area of consistently good data return within the radar view extending beyond the depth of closure (7.27m ODN), where the most significant changes in bathymetry occur.

Figure 6 summarises the stages in data processing used to obtain quality-assured bathymetry from the radar. After the previously defined resolution, *depth-memory* length and quality control procedures were performed, the following data processing steps were applied to create a dataset for further analysis:

- The radar data was filtered to identify records showing calibrated radar-derived $H_s > 1$ m;
- The filtered records were screened to identify periods in which H_s exceeded 1 m for at least 12 hours (24 records). This screening identified the first *data block* in which the *depth memory* had stabilised (i.e. all cell depths within the PDF were calculated from data exceeding the wave height threshold in the previous 12 hours); and
- Bathymetric maps were then produced for each *data block* fitting the criteria stated above. If H_s dropped below the threshold, the *data block* was closed, and a new *data block* initiated when data met the H_s criteria.

During the radar deployment period, 53 *data blocks* were identified using this filtering method. The longest gap between *data blocks* was 80 days (between 06-Mar-2016 and 25-May-2016). Within each *data block* variance in depth was assessed to remove artefacts related to changes in water level, variations in wave direction and nonlinearities in the wave climate across radar field-of-view. Using a bespoke graphical user interface developed in Matlab the *data blocks* were analysed iteratively to identify the records which reflected bathymetric variability commensurate with the multibeam survey data. The bathymetric maps derived from radar data

passing the quality control screening were then analysed to (a) quantify the magnitude and location of significant bathymetric changes, and (b) identify the driving metocean conditions.

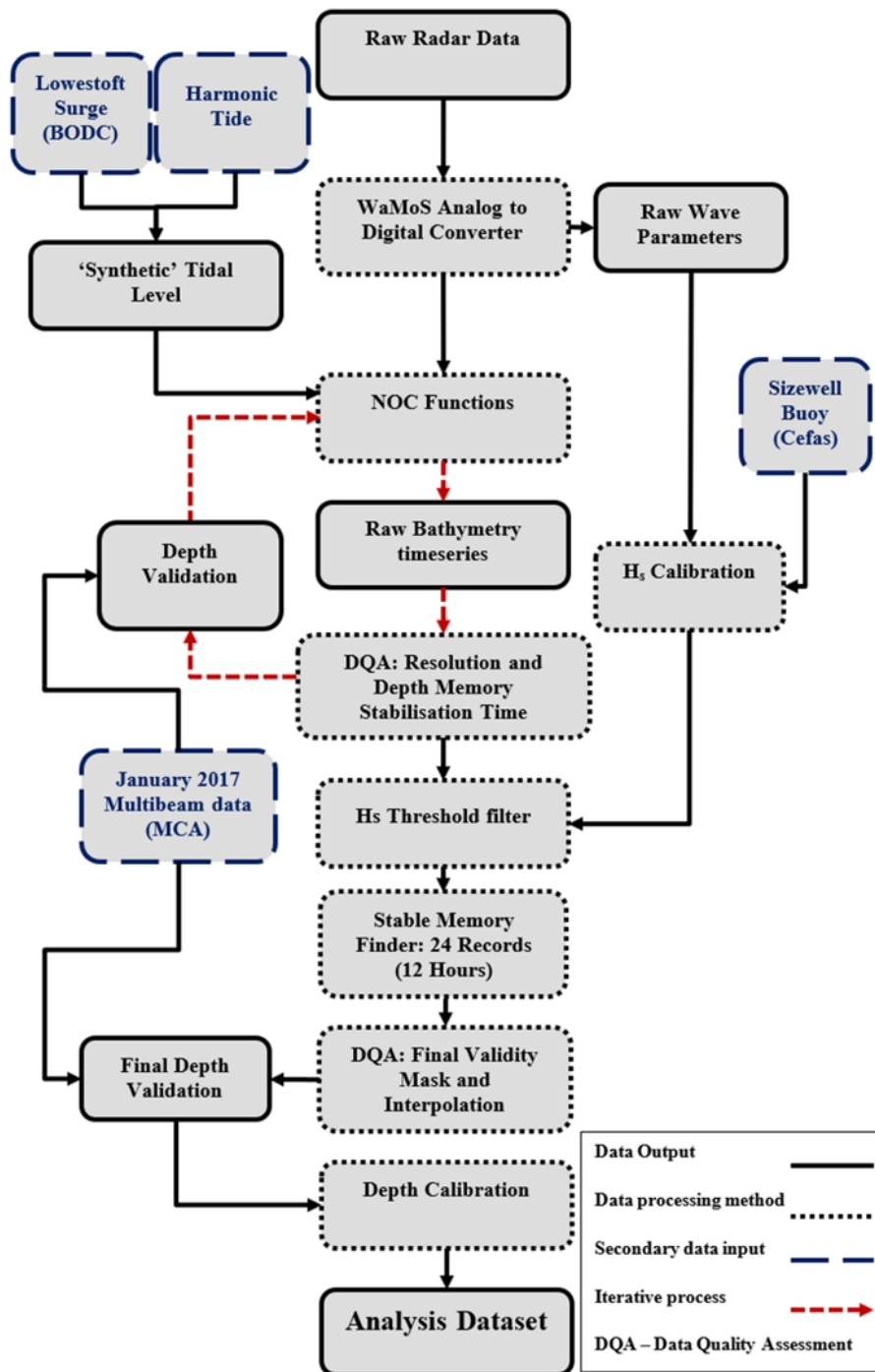


Figure 6. Flow diagram of the data processing and quality control framework employed to produce the radar-derived data.

4 Results

4.1 Validation of radar-derived bathymetry

Figure 7 shows a comparison between bathymetry derived from the radar and measured by multibeam sonar. The results indicate a slight deviation from the line of equivalence whereby shallower depths tend to be overestimated, and deeper depths are underestimated (similar to results reported by Rutten et al. 2017). It is considered that the overestimation of depth by the radar in the shallowest waters is attributable to (a) nonlinearities in wave behaviour in the breaker zone, and (b) the discontinuity of the shore representing the worst-case scenario for violation of the assumption of homogeneity in the data analysis box. The increasing underestimate of depth by the radar in deeper water can be attributed to (a) the dominance of short wavelength and period of waves at the site leading to depth inversion inaccuracy as the wave dynamics become less sensitive to the water depth, (b) inaccuracy in the tidal current correction approach affecting short-wavelength waves (generated by strong local winds) in particular and attributable to vertical current shear.

A comparison between the radar-derived and measured bathymetry showed that 96% of radar-derived values were within ± 0.5 m of the measured data and 100% within ± 1 m of the measured data. Regions initially considered to have the lowest accuracy were confirmed to be the most dynamic with regards to bathymetric changes. These areas included the beach foreshore and a spit-like feature extending south and offshore from the ness. The data conclusively showed that within the resolution constraints defined previously, variability in the radar-derived bathymetry was attributable to the natural changes in sea bed that occurred during the survey period rather than to any uncertainties in the post-processed radar data.

4.2 Identifying areas of near-shore change

The changes in bathymetry recorded by the multibeam surveys enabled discrimination of immobile and mobile seabed areas. With the exception of the areas closest to the shore and across the central sector of the radar view indicated by the black outline in Figure 8, differences between 1 m resolution bathymetry measured by the multibeam survey in 2014 (Figure 8a) and 2017 (Figure 8b) are small or zero within a 1 m resolution (Figure 8c).

Three areas of most significant bathymetric changes are identified as 1, 2, and 3 in Figure 8c and Figure 8d. Area 1 shows distinct erosion (-2 m) of the oblique bar present during the 2014 survey. This erosion is observed to extend north of the ness towards the shoreline and the edge of the radar view. In Area 2 accretion occurs (+2 m) just south of Area 1. There is an abrupt transition between erosion (in Area 1) and accretion (in Area 2). Further offshore of Area 2, narrow bands of erosion and accretion alternate, suggesting a north-westerly migration of large (c. 2 m high, 20-50 m wide) bedforms, such as sand waves, which seem to be constrained by the

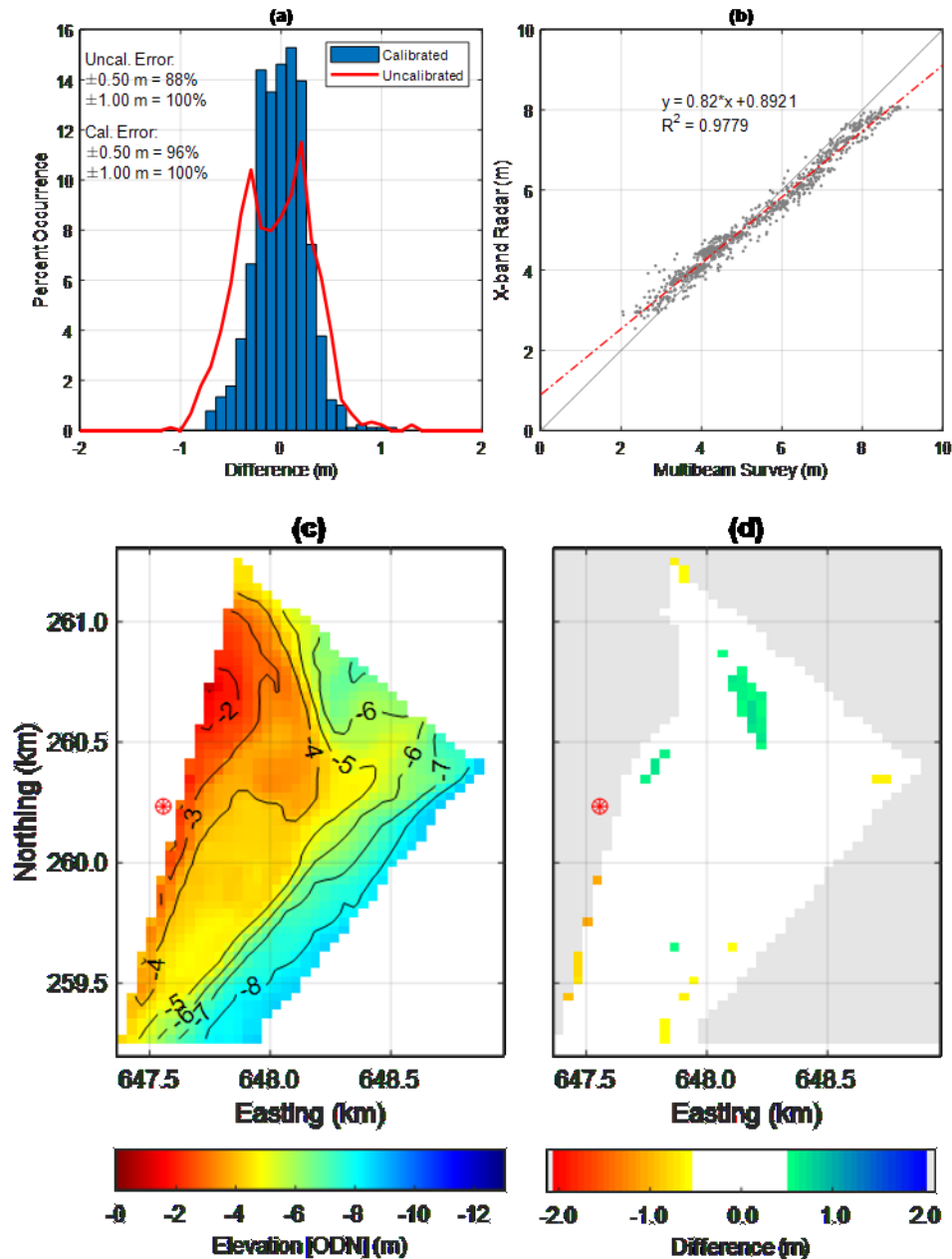


Figure 7. (a) Calibrated radar-derived depths (blue histogram) and uncalibrated depths (red line). (b) Scatter plot of the depths obtained from multibeam surveys and from radar data (uncalibrated) showing the linear regression equation. (c) Radar-derived bathymetry concurrent to the multibeam survey. (d) Differences between multibeam and radar-derived depths, where a negative value indicates an underestimation of the radar and a positive an overestimation.

presence of the Coralline crag ridge (Figure 8c). Although these are the largest changes in bathymetry observed in offshore areas, these features are too narrow to be adequately captured by the radar at the spatial resolution of the wave inversion analysis (Figure 8d) being reduced to one or two result pixels. Area 3 shows significant erosion in the surf zone along most of the southern half of the survey area, including the beach frontage of Thorpeness village.

It is also noted that the apparent bands of erosion (<0.5 m) aligned approximately north-south in the north and south sectors are believed to be artefacts of the surveying method. They

are seen to align with the survey lines (or the trajectory of the vessel) in 2014 and result in a band of erosion that perfectly follows the southeastern edge of the survey coverage, though these changes are well beyond the precision of the radar data.

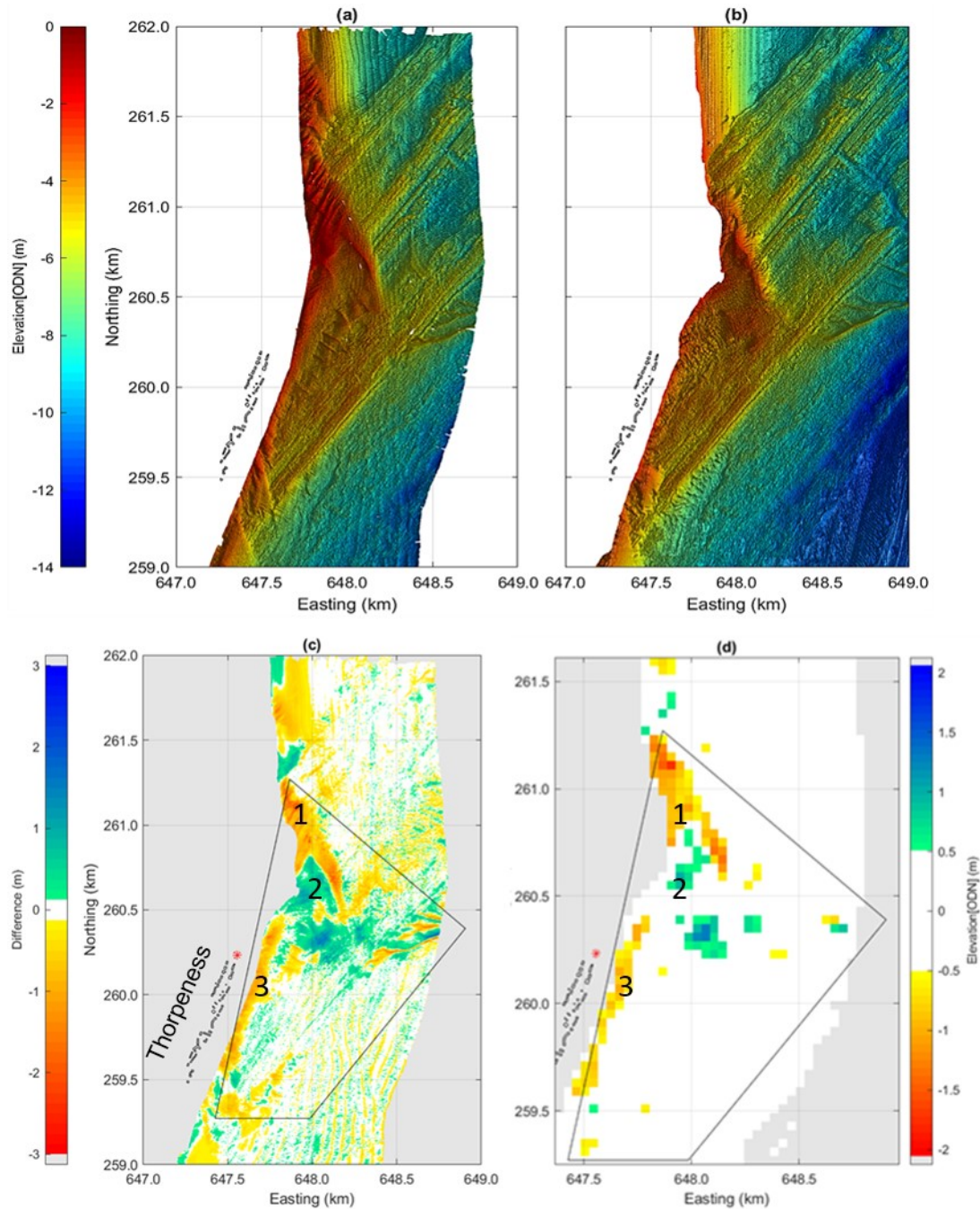


Figure 8. Bathymetry from two multibeam surveys covering the study area obtained (a) by the Environment Agency in June 2014 and (b) by the Maritime Coastal Authority in January 2017. (c) Differences between the two bathymetric maps, where negative values indicate an increase in depth and positive values indicate a reduction in depth (white areas represent changes within the error band ± 0.125 m). (d) Resampling of the map (c) to the same spatial resolution of the radar-derived depth and excluding changes within the error of the radar. The black line boundary indicates the area within the radar view used in the analysis. Thorpeness beach frontage buildings are identified in all figures.

4.3 Quantifying near-shore changes

The present analysis of near-shore bathymetric variability only considered changes exceeding 0.5 m and identified three distinct areas of change based on analysis of the multibeam survey (Figure 9e) including:

- Area 1: an oblique bar north of the radar view extending offshore from the ness;
- Area 2: a region of activity north of the radar and south of the ness; and
- Area 3: a band near the shoreline along the village frontage south of the radar.

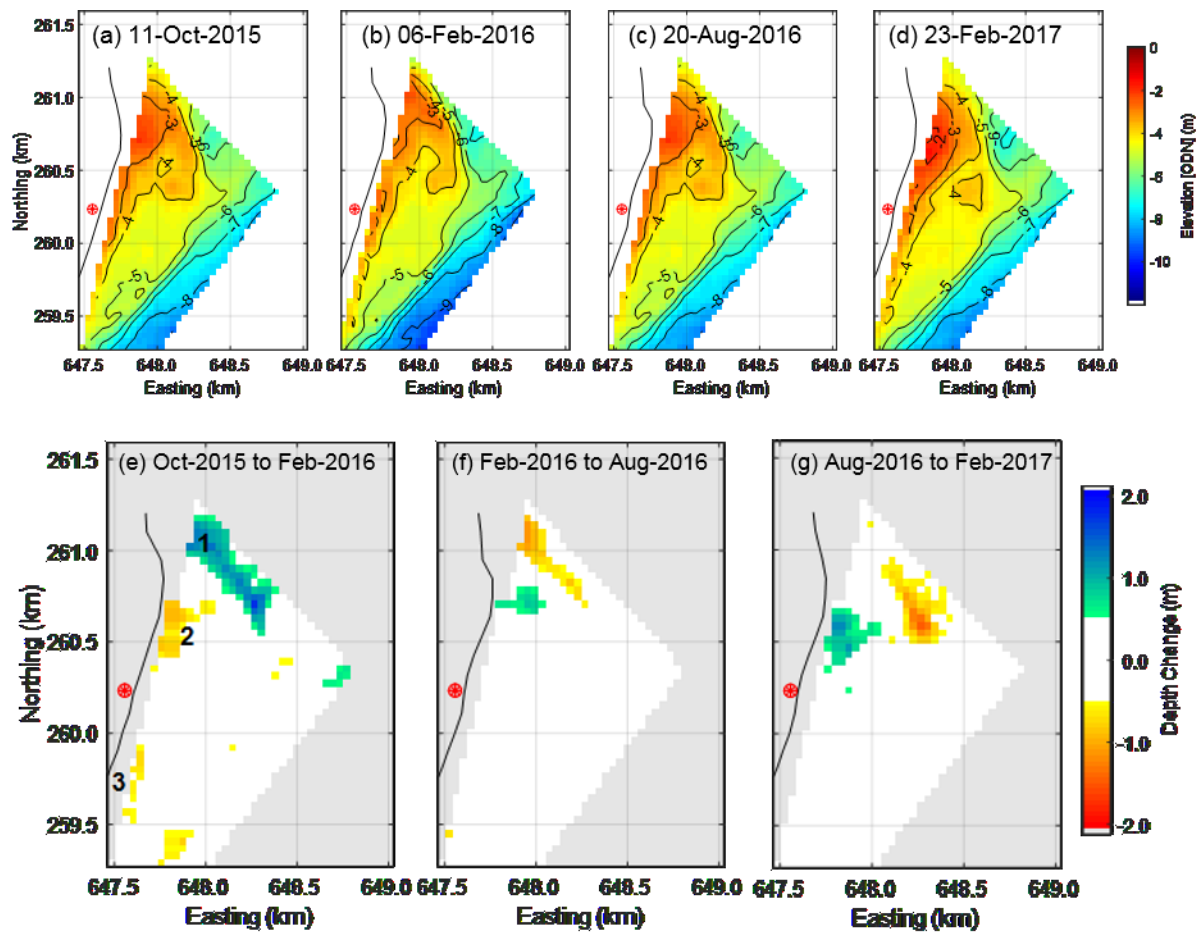


Figure 9. Radar-derived bathymetry of the study area for (a) 11-Oct-2015, (b) 06-Feb-2016, (c) 20-Aug-2016, and (d) 23-Feb-2017 and (e, f, g) maps showing areas of large bathymetric differences (>0.5 m) between these dates. The numbered areas in (e) identify the three areas of largest changes. The red circle indicates radar position. The mean water line is shown as a black line.

Table 1 shows changes in sediment volumes in Areas 1, 2 and 3 for periods of 4 to 6 months (Figure 9) and for periods of 3 to 9 weeks (Figure 10). In common with the temporal differences in sediment volume from the multibeam surveys (Figure 8), analysis of the radar-derived bathymetry show marked changes in sediment volume over 4 to 6 months, particularly in Areas 1 and 2 (Figure 9, Table 1). Here accretion in Area 1 occurred alongside erosion of Area 2 (Figure 9e) and *vice-versa* (Figure 9f,g). Radar-derived data showed that from 11-Oct-2015 to

06-Feb-2016 there was a reduction in the sediment volume in Areas 2 and 3 of 26,063 m³ and 11,653 m³, respectively. During the same period, 112,196 m³ of sediment was added to Area 1 (Table 1), with maximum bathymetric changes reaching +1.75 m and a loss of 11,653 m³ is recorded in Area 3. Between 06-Feb-2016 and 20-Aug-2016, erosion of 36,453 m³ was observed in Area 1 (a maximum bathymetric change of -1.15 m) and accretion of 16,818 m³ occurred in Area 2 (a maximum vertical change of +0.89 m). Although the pattern is a reversal from the previous 6 months, magnitudes of change are considerably lower. During this period a loss of 1,068 m³ is recorded in Area 3. Between 20-Aug-2016 and 23-Feb-2017, erosion intensified in Area 1 with 71,343 m³ of sediment lost. In contrast, Area 2 (Figure 9g) shows accretion of 35,241 m³ and Area 3 remains unchanged.

Table 1. Areas where bathymetric changes exceed radar accuracy (± 0.5 m) and respective estimated changes in sediment volume within longer and shorter periods within the three near-shore areas of interest.

Period		Near-shore change	Area 1		Area 2		Area 3	
			Area [m ²]	Volume [m ³]	Area [m ²]	Volume [m ³]	Area [m ²]	Volume [m ³]
Longer-term changes (4-6 months)								
11-Oct-2015	06-Feb-2016	Accretion	118,400	+112,196				
		Erosion			36,800	-26,063	19,200	-11,653
06-Feb-2016	20-Aug-2016	Accretion			25,600	+16,818		
		Erosion	48,000	-36,453			1,600	-1,068
20-Aug-2016	23-Feb-2017	Accretion			46,400	+35,241		
		Erosion	92,800	-71,343				
Shorter-term changes (3-9 weeks)								
11-Oct-2015	10-Dec-2015	Accretion	72000	+44588	1600	+869		
		Erosion			9600	-6141		
10-Dec-2015	06-Feb-2016	Accretion	67200	+53495				
		Erosion			16000	-8763	17600	-10635
06-Feb-2016	28-Feb-2016	Accretion	6400	+3410	41600	+31116	1600	+884
		Erosion	16000	-9382				

Short-term analysis of sediment volume changes focused on three consecutive periods spanning from October 2015 to February 2016 (Figure 10, Table 1). From 11-Oct-2015 to 10-Dec-2015 (60 days), accretion occurred in Area 1 (44,588 m³) and erosion dominating (6,141 m³) in Area 2 (Figure 10e). This pattern continued and intensified (larger volume changes in less time, Table 1) between 10-Dec-2015 and 06-Feb-2016 when erosion was also observed in Area 3 (Figure 10f). In the following three weeks, accretion in Area 1 subsided and increased considerably in Area 2 reaching magnitudes (31,116 m³) similar to the changes estimated over five months from Aug 2016 to Feb 2017 (Table 1).

The losses and gains in sediment volume presented in Table 1 are conservative and exclude all areas where bathymetric changes were <0.5 m. The magnitudes of bathymetric change over shorter periods are often small, except for a few areas. Consequently, more areas will be excluded from the analysis, resulting in lower estimates of change when compared with analyses that consider more extended periods. This is apparent in Table 1 where the longer-term analysis of change in Area 1 (11-Oct-2015 and 06-Feb-2016) shows accretion of 112,196 m³ and the shorter-term estimates covering the same period show a total accretion of 98,083 m³. This value comprises 44,588 m³ between 11-Oct-2015 and 10-Dec-2015 and 53,495 m³ between 10-

Dec-2015 and 06-Feb-2016. The short-term estimates, therefore, underestimate the volume changes by 14,113 m³ or 12.5 % of the volume. Similarly, a difference of 42% was found between the shorter-term (14,904 m³) and the longer-term (26,083 m³) estimated erosion volume in Area 2.

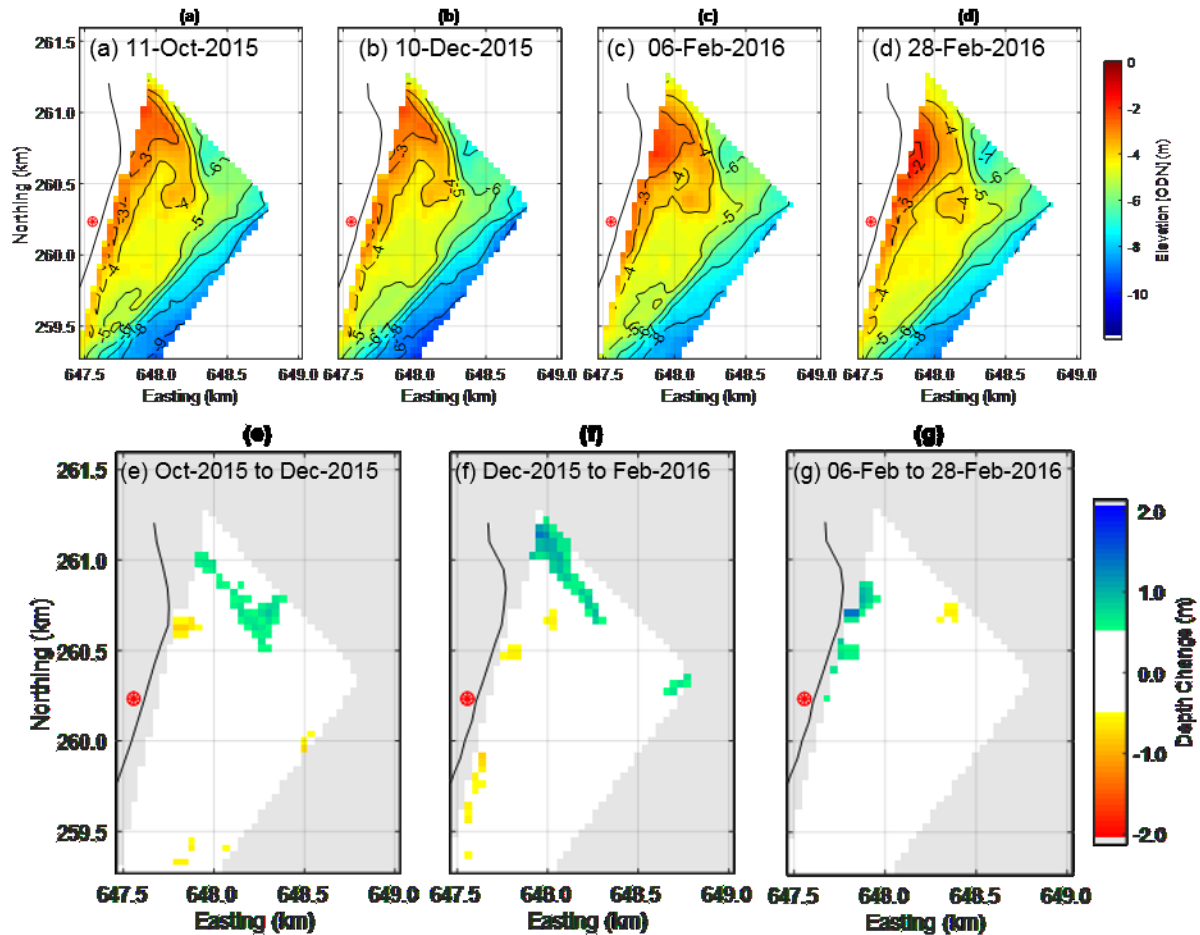


Figure 10. Radar-derived bathymetry of the study area for (a) 11-Oct-2015, (b), 10-Dec-2015, (c) 06-Feb-2016, and (d) 28-Feb-2016 and (e, f, g) maps showing areas of large bathymetric differences (>0.5 m) between these dates. The red circle indicates the radar position. The mean water line is shown as a black line.

6 Discussion

The framework for data quality assessment applied here, includes water level and wave height calibration, ground-truth of radar-derived bathymetry with simultaneous multibeam surveys, and a rigorous selection of data based on optimum site-specific wave conditions. This has enabled for the first-time, quantification of the errors and uncertainties associated with radar-derived bathymetric data and has provided insight into the rates, patterns and volumes of bathymetric changes occurring in the near-shore region.

In accord with work from less complex coastal environments (e.g. Hessner and Bell, 2009; Ludeno et al., 2015), the present work has shown that the accuracy of radar-derived bathymetric obtained during ideal conditions is ± 0.5 m in depths down to 10m. This figure is in line with the higher end of the 5-10% accuracy range quoted by Piotrowski & Dugan (2002) for data originating from an optical system on board a military drone and using similar mathematical

techniques. This accuracy is equivalent to depths extracted from video-systems (Holman et al., 2013) and considerably better than reported from bathymetric lidar (Chust et al., 2010); and satellite data (Li et al., 2019; Traganos et al., 2018). In contrast to Rutten et al. (2017) who showed the greatest accuracy was achieved in water depths greater than 6 m below MSL, this study showed the highest accuracy in shallower waters between 2 to -8 m ODN, with the deeper regions within the radar field-of-view showing significant inaccuracies. It is considered that these differences are attributable to the size of the analysis window (160x160 m in this study and 960x960 m in Rutten et al. 2017).

When compared to other remote sensing techniques, the radar shows greater limitations on the spatial resolution and advantages concerning the range of conditions it can be operational. X-band radar can capture good quality data independently of water transparency (a limitation of bathymetric lidar and satellite data methods), weather conditions and daylight (limitations of video-systems). Further, its range extends beyond that of the camera-based system. Both the video-systems (Holman et al., 1991) and the radar (Bell et al., 2016) enable bathymetric mapping in the intertidal zone using a waterline tracing method. However, the relatively small tidal range and the steepness of the mixed sand-gravel beach at the study site were not conducive to the application of this technique.

The evidence presented here shows that radar can be used as a near-shore monitoring tool, not only for general trends in erosion or accretion but to define also the sediment volume changes in specified areas at a temporal resolution spanning weeks or months. This evidence contrasts with the conclusions of Rutten et al. (2017) who argued that due to substantial bias in shallower regions and to the resolution of the radar, daily to monthly volume changes estimated from radar data are unrealistic. The present accurate near-shore volume change estimates have been made possible in the present study by the analysis framework employed, which focusses on the near-shore region with higher resolution at the cost of data quality loss in deeper water.

In order to put the scale of the observed sediment volume changes into context it is useful to note that the volume change figures for regions 1 and 2 in particular listed in Table 1 for each event are of a similar order of magnitude to the estimated annual longshore sediment transport budget of that part of the coast (Vincent, 1979; Royal Haskoning, 2009). Given that the movement of such large scale sediment features will be dependent on the directional balance, intensity and sequencing of wave events in any given year, it is now intuitively easy to understand how that section of coastline at Thorpeness may be prone to fluctuations in erosion and deposition, which was the underlying reason for deploying the radar system for this project.

5 Conclusions

Using multibeam survey validation data, and robust quality control and data analysis procedures, bathymetric maps have been derived from X-band radar data acquired during an 18-month observational period. The study provides a comprehensive and critical assessment of radar data. It shows that the accuracy of the radar-derived near-shore bathymetry is controlled primarily by the local wave conditions and by the spatial resolution defined in the data analysis methods reported here. Provided wave conditions are suitable, and rigorous data quality control is applied, the radar-derived bathymetry is shown to be accurate to ± 0.50 m down to 10 m water depth at a 40 x 40 m resolution, and changes exceeding this error were measured in time-spans of

weeks. The results obtained in this study would not have been possible using traditional survey methods without an extensive and expensive field monitoring campaign.

During the present radar deployment at Thorpeness, two distinct near-shore morphology states were observed in which seabed features formed and subsequently eroded on time-scales ranging between 4 and 12 months. Modelling reported previously had demonstrated that the location, elevation and spatial extent of these features influenced the incident wave climate along the shoreline of the study area leading to localised erosion hotspots and areas of enhanced accretion. These links between near-shore changes and shoreline evolution could not have been established without recourse to the relatively high temporal and spatial resolution data provided by the radar. The results demonstrate, therefore, the viability of X-Band radar as a cost-effective tool for monitoring near-shore changes in bathymetry along dynamic coasts. This method can provide an early warning of bathymetric changes likely to impact vulnerable coastal locations, thereby allowing coastal managers to mobilise resources that may be required to protect lives and property.

Acknowledgements and Data Availability

This work was conducted as part of John Atkinson's PhD project, co-funded by Bournemouth University, Mott Macdonald and Suffolk Coastal District Council. Radar data used in this research were obtained through the project "X-band radar and evidence-based coastal management decisions" funded by the U.K. Natural Environment Research Council Innovation grant (NE/M021653/1 and NE/M021564/1). The authors would like to thank: Paul Patterson from Coastal Partnership East for his extensive cooperation and support in arranging and dealing with radar installation requirements; Mr Glen Ogilvy for his kind permission for the temporary installation of the radar on his land; Gary Watson at the Environment Agency for facilitating the temporary installation of the pressure sensor in the Thorpeness Sluice; and the support and contribution from Thorpeness residents, particularly: Fred Monson, Mike Chandler, Lucy Ansbro and Mr/Mrs Moore. The authors declare no real or perceived financial conflicts of interests.

All data used in the production of this paper has been banked with the British Oceanographic Data Centre and is available upon request to <https://www.bodc.ac.uk/data> (Ref. BUL200165).

References

- Aarninkhof, S.G.J. & Holman, R.A. (1999), Monitoring the near-shore with video. *Backscatter*, 10(2), 8-11.
- Alpers, W.R., Hasselmann, K., 1982. Spectral signal to clutter and thermal noise properties of ocean wave imaging synthetic aperture radars. *Int. J. Remote Sens.* 3, 423–446.
<https://doi.org/10.1080/01431168208948413>
- Atkinson, J., Esteves, L.S., 2018. Alongshore variability in the response of a mixed sand and gravel beach to bimodal wave direction. *Geosci.* 8. <https://doi.org/10.3390/geosciences8120488>

- Atkinson, J., Esteves, L.S., Williams, J.W., McCann, D.L., Bell, P.S., 2018. The Application of X-Band Radar for Characterization of Nearshore Dynamics on a Mixed Sand and Gravel Beach. *J. Coast. Res.* 85, 281–285. <https://doi.org/10.2112/si85-057.1>
- Bell, P.S., 1999. Shallow water bathymetry derived from an analysis of X-band marine radar images of waves. *Coast. Eng.* 37, 513–527. [https://doi.org/10.1016/S0378-3839\(99\)00041-1](https://doi.org/10.1016/S0378-3839(99)00041-1)
- Bell, P.S., Bird, C.O., Plater, A.J., 2016. A temporal waterline approach to mapping intertidal areas using X-band marine radar. *Coast. Eng.* 107, 84–101. <https://doi.org/10.1016/j.coastaleng.2015.09.009>
- Bell, P.S., Osler, J.C., 2011. Mapping bathymetry using X-band marine radar data recorded from a moving vessel. *Ocean Dyn.* 61, 2141–2156. <https://doi.org/10.1007/s10236-011-0478-4>
- Bell, P.S., Williams, J.J., Clark, S., Morris, B.D., Vila-Concejo, A., 2004. Nested Radar Systems for Remote Coastal Observations. *J. Coast. Res. ICS 2004 Proc. Special Is*, 483–487.
- Borge, J.C.N., Hessner, K., Reichert, K., 1999. Estimation of the Significant Wave Height With X-Band Nautical Radars. *Proc. 18th Int. Conf. Offshore Mech* 1–8.
- Borge, J.C.N.; Rodriguez, G.R.; Hessner, K. & Gonzalez, P.I., 2004. Inversion of Marine Radar Images for Surface Wave Analysis. *Journal of Atmospheric and Oceanic Technology*, 21, 1291-1300.
- Brooks, S.M., Spencer, T., 2012. Shoreline retreat and sediment release in response to accelerating sea level rise: Measuring and modelling cliffline dynamics on the Suffolk Coast, U.K. *Glob. Planet. Change* 80–81, 165–179. <https://doi.org/10.1016/j.gloplacha.2011.10.008>
- Brooks, S.M., Spencer, T., 2010. Temporal and spatial variations in recession rates and sediment release from soft rock cliffs, Suffolk coast, U.K. *Geomorphology* 124, 26–41. <https://doi.org/10.1016/j.geomorph.2010.08.005>
- Browder, A.G., McNinch, J.E., 2006. Linking framework geology and near-shore morphology: Correlation of paleo-channels with shore-oblique sandbars and gravel outcrops. *Mar. Geol.* 231, 141–162. <https://doi.org/10.1016/j.margeo.2006.06.006>
- Burningham, H., French, J., 2017. Understanding coastal change using shoreline trend analysis supported by cluster-based segmentation. *Geomorphology* 282, 131–149. <https://doi.org/10.1016/j.geomorph.2016.12.029>
- Burningham, H., French, J., 2016. Shoreline-Shoreface Dynamics on the Suffolk Coast. CERU Report No. 1608-1, The Crown Estate (2016), ISBN 978-1-906410-76-6, 117 p.
- Burvingt, O., Masselink, G., Russell, P., Scott, T.M., 2017. Classification of beach response to extreme storms. *Geomorphology* 295, 722–737. <https://doi.org/10.1016/j.geomorph.2017.07.022>
- Chust, G.; Grande, M.; Galparsoro, I.; Uriarte, A. & Borja, A., 2010. Capabilities of the bathymetric Hawk Eye LiDAR for coastal habitat mapping: A case study within a Basque estuary. *Estuarine, Coastal and Shelf Science*, 89(3), 200-213. <https://doi.org/10.1016/j.ecss.2010.07.002>
- Costa, B.M.; Battista, T.A. & Pittman, S.J., 2009. Comparative evaluation of airborne LiDAR and ship-based multibeam SoNAR bathymetry and intensity for mapping coral reef ecosystems. *Remote Sensing of Environment*, 113(5), 1082-1100. <https://doi.org/10.1016/j.rse.2009.01.015>

- Davidson, M.A., Van Koningsveld, M., de Kruif, A., Rawson, J., Holman, R.A., Lamberti, A., Medina, R., Kroon, A., & Aarninkhof, S. (2007), The CoastView project: Developing video-derived Coastal State Indicators in support of coastal zone management. *Coastal Engineering*, 54, 463–475. doi.org/10.1016/j.coastaleng.2007.01.007
- Davidson-Arnott, R.G.D., Greenwood, B., 2003. Waves and sediment transport in the near-shore zone, in: *Coastal Zones and Estuaries*. pp. 43–60.
- Deng, A., & Stauffer, D. R. (2006), On improving 4-km mesoscale model simulations. *Journal of Applied Meteorology and Climatology*, 45(3), 361–381. doi:10.1175/JAM2341.1
- Digimap, 2004. Hydroview Reference [WWW Document].
- Dissanayake, P., Brown, J., Wisse, P., Karunarathna, H., 2015. Effects of storm clustering on beach/dune evolution. *Mar. Geol.* 370, 63–75. <https://doi.org/10.1016/j.margeo.2015.10.010>
- Gawehn, M., van Dongeren, A., de Vries, S., Swinkels, C., Hoekstra, R., Aarninkhof, S., Friedman, J., 2020. The application of a radar-based depth inversion method to monitor near-shore nourishments on an open sandy coast and an ebb-tidal delta. *Coast. Eng.* 159, <https://doi.org/10.1016/j.coastaleng.2020.103716>
- Hegermiller, C.A., Rueda, A., Erikson, L.H., Barnard, P.L., Antolinez, J.A.A., Mendez, F.J., 2017. Controls of Multimodal Wave Conditions in a Complex Coastal Setting. *Geophys. Res. Lett.* 44, 12,315-12,323. <https://doi.org/10.1002/2017GL075272>
- Hequette, A., & Aernouts, D. (2010), The influence of near-shore sand bank dynamics on shoreline evolution in a macrotidal coastal environment, Calais, northern France. *Continental Shelf Research*, 30, 1349–1361. doi.org/10.1016/j.csr.2010.04.017.
- Hequette, A., Ruz, M.H., Maspataud, A., & Sipka, V. (2009), Effects Of Nearshore Sand Bank And Associated Channel On Beach Hydrodynamics: Implications For Beach And Shoreline Evolution. *Journal of Coastal Research*, SI56, 59–63.
- Hessner, K., Bell, P.S., 2009. High resolution current & bathymetry determined by nautical X-Band radar in shallow waters. *Ocean. 2009-Europe* 1–5. <https://doi.org/10.1109/OCEANSE.2009.5278333>
- Hessner, K., Reichert, K., Borge, J.C.N., Stevens, C.L., Smith, M.J., 2014. High-resolution X-Band radar measurements of currents, bathymetry and sea state in highly inhomogeneous coastal areas. *Ocean Dyn.* 64, 989–998. <https://doi.org/10.1007/s10236-014-0724-7>
- Hessner, K., Wallbridge, S., Dolphin, T., 2015. Validation of areal wave and current measurements based on X-band radar. *Curr. Waves Turbul. Meas. (CWTM), 2015 IEEE/OES Elev.* 0–9. <https://doi.org/10.1109/CWTM.2015.7098102>
- Holman, R.A.; Sallenger, J.A.H.; Lippmann, T.C. & Haines J.W., 1993. The application of video image processing to the study of near-shore processes. *Oceanography*, 6(3), 78-85. <https://doi.org/10.5670/oceanog.1993.02>
- Holman, R.A., Plant, N., Holland, T., 2013. CBathy: A robust algorithm for estimating near-shore bathymetry. *J. Geophys. Res. Ocean.* 118, 2595–2609. <https://doi.org/10.1002/jgrc.20199>
- Holman, R.A., Stanley, J., 2007. The history and technical capabilities of Argus. *Coast. Eng.* 54, 477–491. <https://doi.org/10.1016/j.coastaleng.2007.01.003>

- Honegger, D.A., Haller, M.C., Holman, R.A., 2019. High-resolution bathymetry estimates via X-band marine radar: 1. beaches. *Coast. Eng.* 149, 39–48.
<https://doi.org/10.1016/j.coastaleng.2019.03.003>
- Honegger, D.A., Haller, M.C., Holman, R.A., 2020. High-resolution bathymetry estimates via X-band marine radar: 2. Effects of currents at tidal inlets. *Coast. Eng.* 156,
<https://doi.org/10.1016/j.coastaleng.2019.103626>
- Koilainen, A.T. & Kaskela, A.M., 2017. Comparison of airborne LiDAR and shipboard acoustic data in complex shallow water environments: Filling in the white ribbon zone. *Marine Geology*, 385, 250-259. <https://doi.org/10.1016/j.margeo.2017.02.005>.
- Kroon, A.; Davidson, M.A.; Aarninkhof, S.G.J.; Archetti, R.; Armaroli, C.; Gonzalez, M.; Medri, S.; Osorio, A.; Aagaard, T.; Holman, R.A. and Spanhoff, R., 2007. Application of remote sensing video systems to coastline management problems. *Coastal Engineering*, 54(6-7), 493-505. <https://doi.org/10.1016/j.coastaleng.2007.01.004>
- Lazarus, E.D. & Murray, A.B., 2011. An integrated hypothesis for regional patterns of shoreline change along the Northern North Carolina Outer Banks, USA. *Marine Geology*, 281, 85-90.
<https://doi.org/10.1016/j.margeo.2011.02.002>.
- Lee, E.M., 2008. Coastal cliff behaviour: Observations on the relationship between beach levels and recession rates. *Geomorphology* 101, 558–571.
<https://doi.org/10.1016/j.geomorph.2008.02.010>
- Lees, B.J., 1983. Sizewell-Dunwich Banks Field Study.
- Li, J.; Knapp, D.E.; Schill, S.R.; Roelfsema, C.; Phinn, S.; Silman, M.; Mascaro, J. & Asner, G.P., 2019. Adaptive bathymetry estimation for shallow coastal waters using Planet Dove satellites. *Remote Sensing of Environment*, 232, 111302.
<https://doi.org/10.1016/j.rse.2019.111302>
- Long, P.E., Zalasiewicz, J.A., 2011. The molluscan fauna of the Coralline Crag (Pliocene, Zanclean) at Raydon Hall, Suffolk, U.K.: Palaeoecological significance reassessed. *Palaeogeogr. Palaeoclimatol. Palaeoecol.* 309, 53–72. <https://doi.org/10.1016/j.palaeo.2011.05.039>
- Lopez, G., Conley, D.C., Greaves, D., 2016. Calibration, Validation, and Analysis of an Empirical Algorithm for the Retrieval of Wave Spectra from H.F. Radar Sea Echo. *J. Atmos. Ocean. Technol.* 33, 245–261. <https://doi.org/10.1175/JTECH-D-15-0159.1>
- Ludeno, G., Reale, F., Dentale, F., Carratelli, E.P., Natale, A., Soldovieri, F., Serafino, F., 2015. An X-band radar system for bathymetry and wave field analysis in a harbour area. *Sensors (Switzerland)* 15, 1691–1707. <https://doi.org/10.3390/s150101691>
- Lund, B., Haus, B.K., Graber, H.C., Horstmann, J., Carrasco, R., Novelli, G., Guigand, C.M., Mehta, S., Laxague, N.J.M., Özgökmen, T.M., 2020. Marine X-band radar currents and bathymetry: An argument for a wave number-dependent retrieval method. *JGR Oceans* 125,
<https://doi.org/10.1029/2019JC015618>
- Masselink, G., Austin, M., Scott, T.M., Poate, T., Russell, P., 2014. Role of wave forcing, storms and NAO in outer bar dynamics on a high-energy, macro-tidal beach. *Geomorphology* 226, 76–93. <https://doi.org/10.1016/j.geomorph.2014.07.025>

- McCann, D.L. & Bell, P.S. 2014. Marine radar derived current vector mapping at a planned commercial tidal stream turbine array in the Pentland Firth, U.K. 2014 *Oceans - St. John's*, <https://doi.org/10.1109/OCEANS.2014.7003186>
- NOC, 2019. POLPRED Technical Information.
- Pacheco, A.; Horta, J.; Loureiro, C. & Ferreira, O., 2015. Retrieval of near-shore bathymetry from Landsat 8 images: A tool for coastal monitoring in shallow waters. *Remote Sensing of Environment*, 159, 102-116. <https://doi.org/10.1016/j.rse.2014.12.004>.
- Piotrowski, C.C. & Dugan, J.C., 2002. Accuracy of bathymetry and current retrievals from airborne optical time-series imaging of shoaling waves. *IEEE TGRS*, 40, 12, 2606 – 2618, <https://doi.org/10.1109/TGRS.2002.807578>
- Pye, K., Blott, S.J., 2006. Coastal Processes and Morphological Change in the Dunwich-Sizewell Area, Suffolk, U.K. *J. Coast. Res.* 223, 453–473. <https://doi.org/10.2112/05-0603.1>
- Reichert, K., Hessner, K., Borge, J.C.N., Dittmer, J., 1999. WaMoS II: A radar based wave and current monitoring system. *Isopé '99 Proc. Vol. 3* 3, 1–5. Royal Haskoning, 2009. Suffolk SMP2 Sub-cell 3c Review of coastal processes and Geomorphology. Draft Report. Suffolk Coastal District Council. Report RCP1/301164/PBor.
- Ruessink, B.G., Van Enckevort, I.M.J., Kuriyama, Y., 2004. Non-linear principal component analysis of near-shore bathymetry. *Mar. Geol.* 203, 185–197. [https://doi.org/10.1016/S0025-3227\(03\)00334-7](https://doi.org/10.1016/S0025-3227(03)00334-7)
- Rutten, J., de Jong, S.M., Ruessink, G., 2017. Accuracy of Nearshore Bathymetry Inverted From X-Band Radar and Optical Video Data. *IEEE Trans. Geosci. Remote Sens.* 55, 1106–1116. <https://doi.org/10.1109/TGRS.2016.2619481>
- Schupp, C.A., McNinch, J.E., List, J.H., 2006. Near-shore shore-oblique bars, gravel outcrops, and their correlation to shoreline change. *Mar. Geol.* 233, 63–79. <https://doi.org/10.1016/j.margeo.2006.08.007>
- Senet CM, Seemann J, Ziemer F (2001) The near-surface current velocity determined from image sequences of the sea surface. *IEEE Trans Geosci Remote Sens* 39(3):492–505 <https://doi.org/10.1109/36.911108>
- Sibson, R., 1981. *Interpolating Multivariate Data*. John Wiley, Chichester.
- Smit, M.W.J., Aarninkhof, S.G.J., Wijnberg, K.M., Gonzalez, M., Kingston, K.S., Southgate, H.N., Ruessink, B.G., Holman, R.A., Siegle, E., Davidson, M.A., Medina, R., 2007. The role of video imagery in predicting daily to monthly coastal evolution. *Coast. Eng.* 54, 539–553. <https://doi.org/10.1016/j.coastaleng.2007.01.009>
- Stewart, R.H. and J.W. Joy, 1974. H.F. radio measurement of surface currents. *Deep-Sea Research* 21, 1039-1049. [https://doi.org/10.1016/0011-7471\(74\)90066-7](https://doi.org/10.1016/0011-7471(74)90066-7)
- Stokes, C., Davidson, M.A., Russell, P., 2015. Observation and prediction of three-dimensional morphology at a high-energy macrotidal beach. *Geomorphology* 243, 1–13. <https://doi.org/10.1016/j.geomorph.2015.04.024>

Traganos, D.; Poursanidis, D.; Aggarwal, B.; Chrysoulakis, N. & Reinartz, P., 2018. Estimating Satellite-Derived Bathymetry (SDB) with the Google Earth Engine and Sentinel-2. *Remote Sensing*, 10(6), 859, <https://doi.org/10.3390/rs10060859>.

Vincent, C.E., 1979. Longshore sand transport rates—a simple model for the East Anglian coastline. *Coast. Eng.* 3, 113–136.

Wadey, M.P., Haigh, I.D., Nicholls, R.J., Brown, J.M., Horsburgh, K., Carroll, B., Gallop, S.L., Mason, T., Bradshaw, E., 2015. A comparison of the 31 January–1 February 1953 and 5–6 December 2013 coastal flood events around the U.K. *Front. Mar. Sci.* 2. <https://doi.org/10.3389/fmars.2015.00084>.

Williams, J.J., 2014. Thorpeness Coastal Erosion Appraisal, Mott MacDonald.

Williams, J.J.; Atkinson, J.; Price, D.M.; Esteves, L.S. & Costa, S.S., 2019. New understanding of a coastal erosion hotspot in a bimodal wave climate. *Coastal Sediments '19*, 817-829. DOI: 10.1142/9789811204487_0072.

Wyatt, L.R., Green, J.J., Gurgel, K.W., Borge, J.C.N., Reichert, K., Hessner, K., Günther, H., Rosenthal, W., Saetra, O., Reistad, M., 2003. Validation and intercomparisons of wave measurements and models during the EuroROSE experiments. *Coast. Eng.* 48, 1–28. [https://doi.org/10.1016/S0378-3839\(02\)00157-6](https://doi.org/10.1016/S0378-3839(02)00157-6).